Monitoring sinew contraction during formation of tissue-engineered fibrin-based ligament constructs.

Paxton, Jennifer; Wudebwe, Uchena; Wang, A; Woods, D; Grover, Liam

DOI:
10.1089/ten.TEA.2011.0535

Document Version
Publisher's PDF, also known as Version of record

Citation for published version (Harvard):
Paxton, J, Wudebwe, U, Wang, A, Woods, D & Grover, L 2012, 'Monitoring sinew contraction during formation of tissue-engineered fibrin-based ligament constructs.', *Tissue Engineering Part A*, vol. 18, no. 15-16, pp. 1596-1607. https://doi.org/10.1089/ten.TEA.2011.0535

TISSUE ENGINEERING: Part A
Volume 18, Numbers 15 and 16, 2012

DOI: 10.1089/ten.tea.2011.0535

Monitoring Sinew Contraction During Formation of Tissue-Engineered Fibrin-Based Ligament Constructs

Jennifer Z. Paxton, Ph.D.,[1] Uchena N.G. Wudebwe, M.Eng.,[1] Anqi Wang, Ph.D.,[1,2]
Daniel Woods, Ph.D.,[3] and Liam M. Grover, Ph.D.[1]

The ability to study the gross morphological changes occurring during tissue formation is vital to producing tissue-engineered structures of clinically relevant dimensions *in vitro.* Here, we have used nondestructive methods of digital imaging and optical coherence tomography to monitor the early-stage formation and subsequent maturation of fibrin-based tissue-engineered ligament constructs. In addition, the effect of supplementation with essential promoters of collagen synthesis, ascorbic acid (AA) and proline (P), has been assessed. Contraction of the cell-seeded fibrin gel occurs unevenly within the first 5 days of culture around two fixed anchor points before forming a longitudinal ligament-like construct. AA + P supplementation accelerates gel contraction in the maturation phase of development, producing ligament-like constructs with a higher collagen content and distinct morphology to that of unsupplemented constructs. These studies highlight the importance of being able to control the methods of tissue formation and maturation *in vitro* to enable the production of tissue-engineered constructs with suitable replacement tissue characteristics for repair of clinical soft-tissue injuries.

Introduction

In vitro engineering of connective tissues for surgical implantation is an active field of research. In particular, the manufacture of suitable artificial tissues for replacement of the anterior cruciate ligament (ACL) is receiving much interest, as each year an estimated 80,000 to 100,000 ACL ruptures occur in the United States alone.[1] The majority of these injuries occur in young, active individuals,[2] and failure to repair the injured tissue will result in joint instability,[3] pain,[1] injury to other structures within the knee joint,[3] muscle weakness,[4] and the subsequent development of osteoarthritis.[5,6] While attempts have been made to repair the ACL with synthetic graft replacements (e.g., Gore-tex, Dacron, and carbon fibers), problems resulting from the mechanical breakdown of the grafts mean that transplantation of an autograft to the injured site remains the most successful method of ACL repair. However, because of problems such as pain,[7,8] muscle weakness,[4] patellar tendonitis,[9] and donor-site morbidity[10] after autograft treatment, tissue-engineered constructs are now being investigated for implantation.

We have recently shown that complete bone-ligament-bone constructs for potential implantation and repair of the ACL can be formed *in vitro* using brushite anchors and a cell-seeded fibrin gel.[11] However, little attention has been given to the three-dimensional (3D) morphology of the soft-tissue portion of the graft during construct formation and the effects of anabolic supplementation on morphology. Such information is desirable to predict the long-term size and shape of construct grafts for implantation. While conventional imaging techniques, such as histology, usually allow only visualization of the tissue using destructive methods, we have used the nondestructive optical coherence tomography (OCT) imaging technology alongside conventional digital imaging to visualize the morphology of constructs during their formation and maturation phases.

OCT is an emerging imaging technology for the biological and medical sciences. It enables imaging of 1–2-mm inside opaque tissue without any special preparation, making it an ideal nondestructive adjunct to histology. Also, the use of low-power infrared light means that OCT is also noncontact, noninvasive, and capable of providing high-resolution images at a video rate. OCT works by focusing a beam of light inside a sample, and the depth positions of multiple subsurface structures are then determined by performing frequency-domain time-of-flight measurements on the back-scattered light, resulting in a tomographic depth-reflectivity profile (A-scan). One- and two-dimensional (2D) scanning of

[1]School of Chemical Engineering, College of Physical Sciences and Engineering, University of Birmingham, Edgbaston, Birmingham, United Kingdom.
[2]School of Dentistry, College of Medical and Dental Sciences, University of Birmingham, St Chad's Queensway, Birmingham, United Kingdom.
[3]Michelsons Diagnostics, Orpington, Kent, United Kingdom.

the focused beam can then be used to make 2D and 3D images of the sample. Recently, OCT has been used within many different fields of research from cancer biology[12,13] and development[14–16] to clinically within cardiology[17] and ophthalmology[18–20] owing to the nondestructive nature of the technique and the ability to visualize inside tissues and organisms. Furthermore, it has also received great attention within the tissue engineering field, having been described as a technique with great promise for visualizing engineered tissues.[21] Many groups have utilized this imaging technique to study scaffold morphologies,[21–26] collagen gel remodeling,[27] and collagen fiber alignment.[28]

The aim of this study was to investigate the morphological changes occurring during the early-stage formation and maturation of tissue-engineered bone-to-bone ligament-like constructs manufactured from fibroblast-seeded fibrin gels. Digital imaging, OCT, and histological techniques were used to evaluate construct development over time.

Materials and Methods

β-Tricalcium phosphate manufacture

The β-tricalcium phosphate (β-TCP; $Ca_3(PO_4)_2$) was manufactured by reactive sintering of a powder containing $CaHPO_4$ (Mallinckdrodt-Baker) and $CaCO_3$ (Merck), with a theoretical calcium to phosphate molar ratio of 1.5. The powder mixture was suspended in absolute ethanol and mixed for 12 h. After this, the suspension was filtered and the resulting cake heated in an alumina crucible to 1400°C for 12 h and 1000°C for 6 h before quenching in a dessicator in ambient conditions. The resulting sinter cake was then crushed using a pestle and a mortar, and was passed through a 125-μm sieve.

Brushite cement formation

The brushite cement was made by incrementally combining β-TCP ($Ca_3(PO_4)_2$) with 3.5 M orthophosphoric acid (H_3PO_4; Sigma-Aldrich) at a ratio of 3.5 mg/mL to form a paste. Citric acid (200 mM; Sigma-Aldrich) and sodium pyrophosphate (200 mM; Sigma-Aldrich) were added to the H_3PO_4 before combination with β-TCP. The paste was consolidated into a custom-made silicone mold,[29] and mold-filling was improved with the use of a vibrating platform (Denstar 500; National Dental Supplies) for 60 s. Stainless steel insect pins (0.2-mm diameter; Fine Science Tools) were inserted into each anchor before setting occurred, and cement anchors were left to set within their molds overnight at 37°C. Final cement anchors were trapezoidal in shape, measuring $\sim 4 \times 4$ mm at the widest points and 3 mm in height as described previously.[11,29]

Ligament-like construct formation

Thirty-five-millimeter Petri dishes were coated with 1.5 mL of Sylgard (type 184 silicone elastomer; Dow Corning Corporation) and left to polymerize for at least a week before use. Cement anchors were removed from their molds and pinned to the sylgard layer ~ 12 mm apart, and the anchors and plate were sterilized by soaking in 70% ethanol for 20 min. The Sylgard layer was used to allow immobilization of the cement anchors and to provide a non-cell-adhesive surface underneath the fibrin gel. Five hundred microliters of the Dulbecco's modified Eagle's medium (DMEM; Invitrogen) supplemented with 10% fetal bovine serum (FBS; Biosera), 1% penicillin/streptomycin (P/S; Invitrogen), 50 U/mL thrombin (Calbiochem), 400 μM aminohexanoic acid (Sigma-Aldrich, UK), and 20 μg/mL aprotinin (Roche) solution was used to coat the Sylgard layer. Two hundred microliters of 20 mg/mL fibrinogen (Sigma-Aldrich) was then added dropwise, and the fibrin gel was left to polymerize at 37°C for 1 h. Embryonic chick tendon fibroblasts were isolated from the flexor tendons of 13.5-day-old chick embryos by a 1.5-h digestion in the collagenase type-II solution (in serum- and antibiotic-free DMEM) at 37°C. After digestion, the solution was passed through a 100-μm cell strainer (BD Biosciences) to remove any insoluble material. The cell solution was spun at 2500 rpm for 3 min. The resulting cell pellet was suspended in the DMEM supplemented with 10% FBS and 1% P/S (Invitrogen). Chick tendon fibroblasts were cultured and split routinely, and used between passages 2 and 5. Cells were seeded on top of the polymerized fibrin gel at a concentration of 100,000 cells in 1 mL. The growth medium (DMEM + 10% FBS + 1% P/S) was replenished on day 3 after seeding, and then every 2–3 days for the duration of the experiments. On day 7 of formation, half the ligament-like constructs received supplementation with 250 μM ascorbic acid 2-phosphate (AA; Sigma-Aldrich) and 50 μM L-proline (P; Sigma-Aldrich) added to the growth medium. Day 7 was chosen, as it was in line with previous work.[11,29] This supplementation regime was continued on every day of medium replenishment in the AA + P-treated samples. Over time, the fibrin gel contracts around the two brushite cement anchors to form a cement-cellularized fibrin gel–cement (bone-ligament-bone) construct.

Optical coherence tomography

Ligament-like constructs were scanned using a high-resolution EX1301 MultiBeam OCT microscope daily from day 0 to day 7, followed by day 10, day 14, and then every 7 days until day 35 ($n = 16$ in each treatment group). The day-0 scans were taken after the addition of cells in the growth medium. The microscope was equipped with a Santec HSL-2010 swept-source laser with a spectral range of 150 nm spectrum centered at 1310 nm. The measured resolution was < 9 μm axially (depth) and < 7.5 μm laterally. The frequency of A-scans was at a rate of 10,000/s. Optical B-Scans comprising 1188 A-Scans and spanning ~ 5 mm laterally and 1.9 mm in depth (1188×460 pixels) were captured showing cross sections of the ligaments in the longitudinal orientations. For transverse orientations, B-scans comprised 242–1118 A-scans depending on the diameter of the construct at the time of scanning. Multiple parallel B-Scan image sets with fixed spatial periodicity were also acquired by moving the sample orthogonally to the B-Scan direction on an automated translation stage in 4-μm steps. Using this technique, 3D volumes of ligament-like constructs can be digitally reconstructed with dimensions up to $5 \times 25 \times 1.9$ mm for fly-through examination. Constructs were scanned in their Petri dishes, in the growth medium, with the Petri dish lid removed. Consequently, each sample could only be used for one time point per scan. Images of the constructs were also taken using a digital camera (Optio V10; Pentax Corporation) at the same time points as the scans. Constructs that have not been assigned for time-point scans were kept in

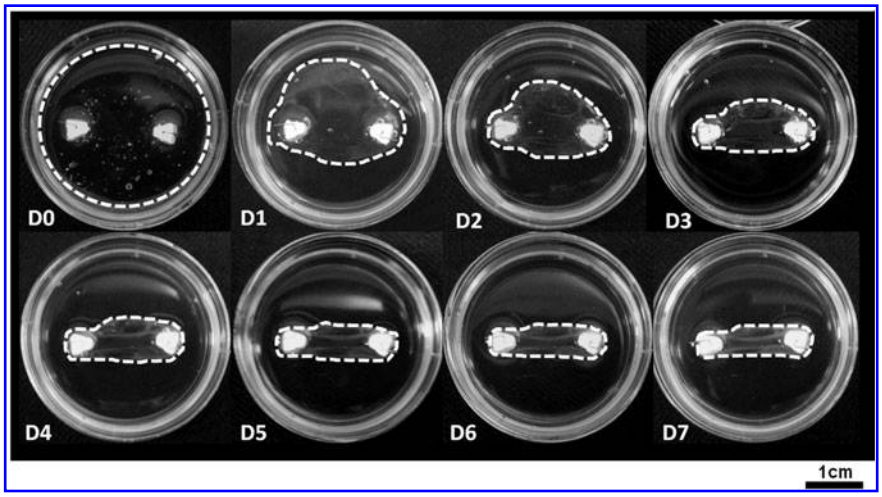

FIG. 1. Early-stage formation of the ligament-like constructs. Digital images of the constructs were taken each day from day 0 (D0) to day 7 (D7) after cell seeding. The outer edges of the fibrin gel have been marked for clarity (white-dashed line). Over the course of the 7 days, the fibrin gel contracts unevenly around the two fixed anchor points. Constructs are formed in 35-mm Petri dishes.

the same culture conditions until the 2.5-month time point, where 3D scans were taken ($n=1$ each condition).

Gel contraction analysis

To investigate and quantify the effect of supplementation with AA+P on gel contraction, constructs were formed and supplemented with or without AA+P from day 0 of culture ($n=7$ in each group). The decision to supplement from day 0 was to investigate the effect of AA+P on gel contraction from the beginning of formation, rather than from day 7 as described earlier. Digital images were taken of each construct every day until day 15, and then every other day thereafter. Gel surface areas were quantified using image analysis software (ImageJ; NIH) to calculate percentage reduction in gel area over time. Further to this, the maximum and minimum widths of the ligament-like constructs transverse to the longitudinal length were also measured ($n=7$ in each group; ImageJ; NIH.). All measurements were taken in between the anchors to ensure consistency.

Histology

The ligament-like constructs were removed from their culture media at the 5-week and 10-week time points ($n=2$) and fixed in 4% formaldehyde buffer in phosphate-buffered saline at 4°C for 24 h. Samples were then dehydrated in a series of ethanol solutions from 35% to 100% followed by 100% xylene. The specimen was then transferred to a 60°C paraffin wax bath (HISTO WAX 514409) overnight, and then placed under vacuum (Citadel 1000; Thermo Shandon) for 4 h to allow wax infiltration. The sample was later embedded in paraffin wax, and a LEICA RM 2035 microtome was used to cut 5–7-μm sections. The sections were picked up on glass coverslips (four per slide and two slides per construct) that were left in a 60°C oven for 30 min before they were stained using hematoxylin and eosin (H&E; SHANDON Linistain GLX) per the manufacturer's instructions. Stained sections were viewed on a light microscope (Inverso 3000, Ceti; Progen Scientific) and images taken using Image Capture (Ceti; Progen Scientific).

Collagen content

The collagen content of ligament-like constructs was measured over time using a hydroxyproline assay, as hydroxyproline accounts for ~13% of total collagen and is released after tissue hydrolysis.[30,31]

Briefly, ligament constructs ($n=4$ each time point and group) were removed from their cement anchors and left to dehydrate at 37°C for at least 72 h. The dry mass of each sample was then measured, and the dry sample was hydrolyzed in 200 μL of 6 M HCl at 130°C for 3 h. The liquid was removed by allowing the HCl to evaporate for 30 min in a fume hood at 130°C. The resulting pellet was re-suspended in 200 μL of hydroxyproline buffer. Samples were further diluted 1:8 in hydroxyproline buffer. About 150 μL of chloramine T solution was added to each sample, vortexed, and left at room temperature for 20 min. About 150 μL of aldehyde–perchloric acid solution was then added to each tube before the tubes were vortexed and incubated in a preheated water bath at 60°C for 15 min. After incubation, tubes were left to cool for 10 min, and then samples/standards were read at 550 nm on a Glomax Multi Detection System Plate reader (Promega). Hydroxyproline was converted to collagen using a factor of 13.34%.

Statistical analysis

Where appropriate, data are presented as means ± standard error of the mean. Differences in mean values were compared within groups, and significant differences were determined by analysis of variance with the *post hoc* Tukey-Kramer Honestly Significant Difference test using BrightStat.[32] The significance level was set at $p<0.05$. The gel contraction data were analyzed using independent one-tailed tests (IBM SPSS Statistics 19) on a day-by-day basis. To determine the effect size of the data, Pearson's correlation r was used such that r values <0.1 represented a small effect; 0.3, a medium effect; and 0.5 or greater, a large effect. The Cohen's d method was also used, with categories being 0.2 is small, 0.5 is medium, and 0.8 is large. Pearson's r and Cohen's d effect sizes are referred to as ES r and ES d, respectively. *Post hoc* power analyses were also conducted (DSS Research Statistical Power Calculator).

Results

Early-stage formation of ligament-like constructs

Over the course of 7 days, the cell-seeded fibrin gel contracted around the two fixed brushite anchor points (Fig. 1).

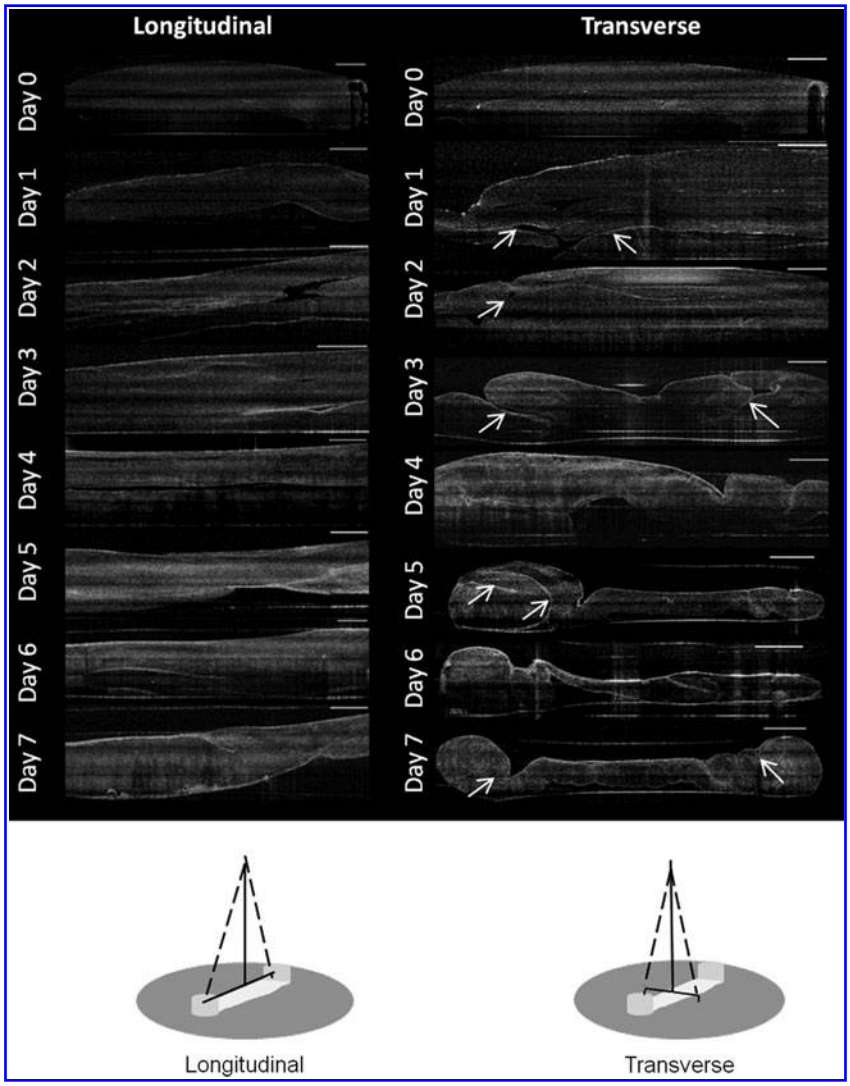

FIG. 2. Optical coherence tomography (OCT) scans in the longitudinal and transverse orientations during early-stage formation of the ligament-like constructs. OCT scans were performed daily. Fibrin gel contraction is evident from day 1 after cell seeding and continues over the course of the week. Folds in the fibrin gel are marked with arrows. Scale bar represents 1 mm in all images. Schematic diagrams depict the scanning direction in both orientations.

The fibrin gel began to contract rapidly and unevenly within 5 days after cell seeding, continuing rapid contraction until day 5, when the contraction rate noticeably reduced (Fig. 1).

The OCT scans demonstrate the method of gel contraction in the ligament constructs. Folds of the fibrin gel can be seen in the transverse scans from day 1 onward (Fig. 2, arrows), becoming clearly evident at day 3 (Fig. 2). The uneven nature of gel contraction demonstrated in Figure 1 can also be observed in Figure 2. By day 7, both sides of the fibrin gel have contracted around the anchor points evenly, and the folds have coalesced into a single solid mass (Figs. 1 and 2).

Maturation of ligament-like constructs

Contraction of the ligament constructs continues over several weeks of maturation (Fig. 3). Supplementation of the

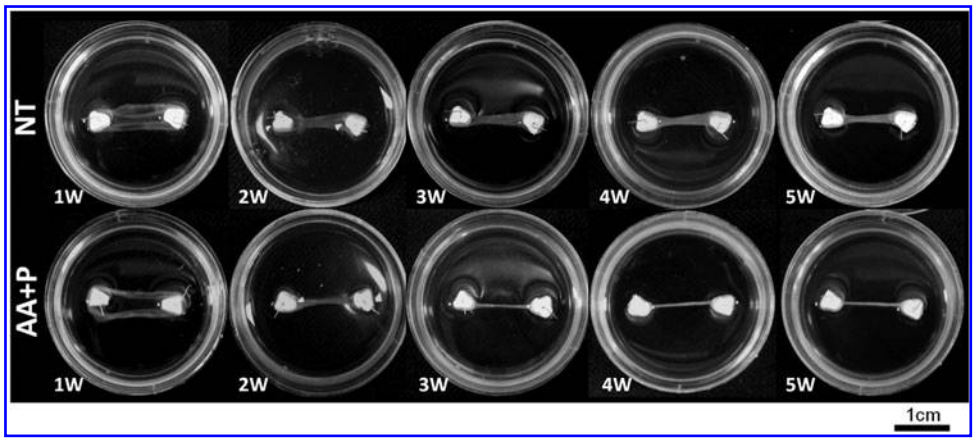

FIG. 3. Maturation of the ligament-like constructs. Digital images of the ligament-like constructs over a 5-week period in unsupplemented and supplemented groups (250 μM ascorbic acid 2-phosphate [AA] + 50 μM proline [P]). Supplementation causes increased contraction from week 2 (2W) onward. Constructs are formed in 35-mm Petri dishes. NT, no treatment.

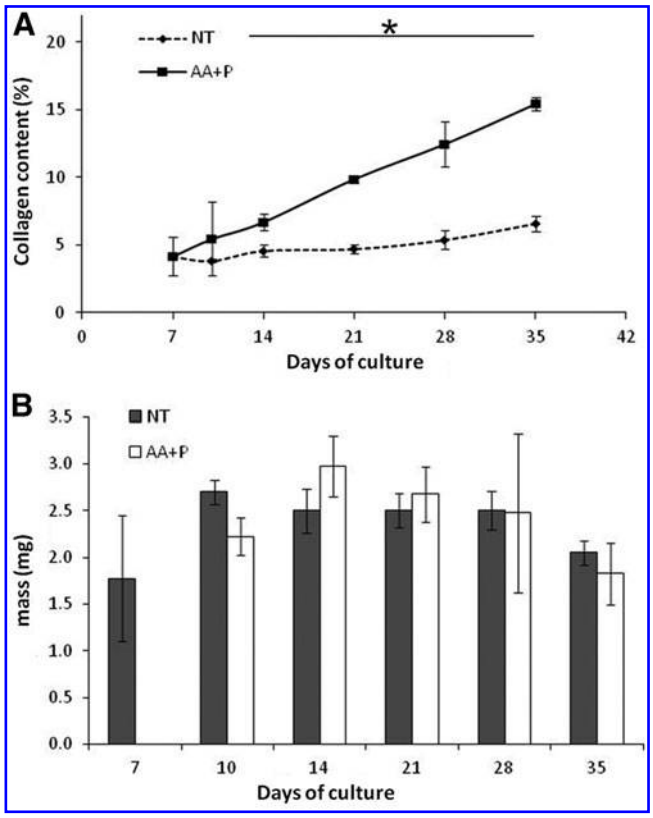

FIG. 4. Collagen content of ligament-like constructs. **(A)** AA+P causes a significant increase in the collagen content when compared to unsupplemented samples at all time points from 14 days. $*p<0.05$ when compared to the unsupplemented group. $n=6$ in all groups. **(B)** Dry mass of constructs does not significantly differ between supplemented and unsupplemented groups. $n=6$ in all groups.

culture medium with AA+P has a marked effect on contraction of the constructs, with supplemented constructs continuing to contract beyond the boundaries of the cement anchors as seen in the unsupplemented group (Fig. 3). Notably, in both the unsupplemented and supplemented groups, the constructs became white and appeared to increase in opacity over time, which is indicative of increased matrix deposition in the samples (Fig. 3). To confirm this, the hydroxyproline content constructs were measured at each time point (Fig. 4). As anticipated, the supplemented group continued to produce collagen, with the collagen content rising significantly from 4.16%±1.42% at 1 week to 15.45%±0.49% per construct after 5 weeks of culture ($p>0.00$). In the unsupplemented samples, however, the collagen content stayed relatively constant, with no significant difference observed between week 1 and week 5 of culture at any time point measured ($p>0.05$ at all time points). Furthermore, the dry weights of the constructs do not significantly differ at any time point measured (Fig. 4B).

Figure 5A displays the longitudinal scans of the constructs using OCT in the maturation phase of development. Over the course of 5 weeks, the constructs became thinner and more opaque, markedly so in the AA+P-treated samples (Fig. 5A). The transverse scans of the constructs clearly demonstrated gross morphological changes occurring during construct maturation (Fig. 5B). In both the AA+P-treated samples and the unsupplemented group, the constructs display a rolled-up appearance after 1 week of formation. Gradually, the two sides of the construct contracted and joined to form a tubular structure by week 2 (Fig. 5B). Notably, this occurred faster in the AA+P-treated group (Fig. 5B). Cross-sectional areas of the transverse OCT scans were measured and plotted against time (Fig. 5C). At all time points after 14 days, unsupplemented samples possess a larger cross-sectional area than supplemented constructs (Fig. 5C), reaching significance on day 14 ($p=0.001$), day 28 ($p=0.01$), and day 35 ($p=0.0001$). Over the course of the following weeks, constructs in both groups contracted further, became more opaque, and displayed a more uniform tissue distribution. Continued culture of the ligament-like constructs for several months in culture maintains this gross morphology as shown in the 3D reconstructions of constructs with dense constructs with distinct morphologies produced (Fig. 6). As shown previously in the digital images (Fig. 3), constructs in the AA+P-treated group underwent significant contraction, becoming <2 mm in width by 4 weeks of culture. To investigate the effect of supplementation of AA+P on the contraction of cell-seeded fibrin gels, constructs were photographed every day after cell seeding for 2 weeks and then every other day for the duration of the experiment. Gel areas were then calculated using digital imaging software (ImageJ; NIH). The percentage reduction in the gel area is displayed in Figure 7. Overall, it appears that supplementation has no prominent effect on gel contraction. However, to allow for better comparison of the gel contraction, percentage area reductions were plotted for specific time periods of the experiment—the early-stage contraction period (0–7 days, Fig. 7B), maturation of the ligament-like constructs (7–35 days, Fig. 7C), and late-stage maturation (35–52 days, Fig. 7D). Figure 7B demonstrates that at the initial stage of gel contraction, unsupplemented constructs contract faster than supplemented, reaching a similar gel area by 7 days. Unsupplemented constructs contract to 40.83%±4.12% of their original area in the first 24 h after seeding (Fig. 7B) compared to AA+P-supplemented reduction to 45.52%±4.95%. Conversely, as contraction continues after day 7, AA+P-supplemented constructs display a faster rate of contraction with the difference between groups stabilizing at around day 14 (Fig. 7C). The most noticeable difference between groups is observed in the late-stage formation of ligament-like constructs, where from day 33 to day 36, AA+P-supplemented constructs contract more and then exhibit a smaller area at the remaining time points, with values of 2.72%±0.11% and 3.41%±0.47%, respectively (Fig. 7D). Statistical analysis revealed that while this difference was not significant ($p>0.05$), it represented a large effect size (an indication of the strength of the relationship between the groups).[33,34]

To further quantify the differences observed between the constructs, the maximum and minimum transversal widths were measured. As with the construct gel area measurements, the largest change in widths was observed between day 0 and day 1 (Fig. 8). The no treatment (NT) group exhibited a greater extent of contraction in comparison to the AA+P group. The maximum width of the NT constructs reduced from 35 to 13.98±4.45 mm, and the maximum width of the AA+P supplemented maximum width reduced to

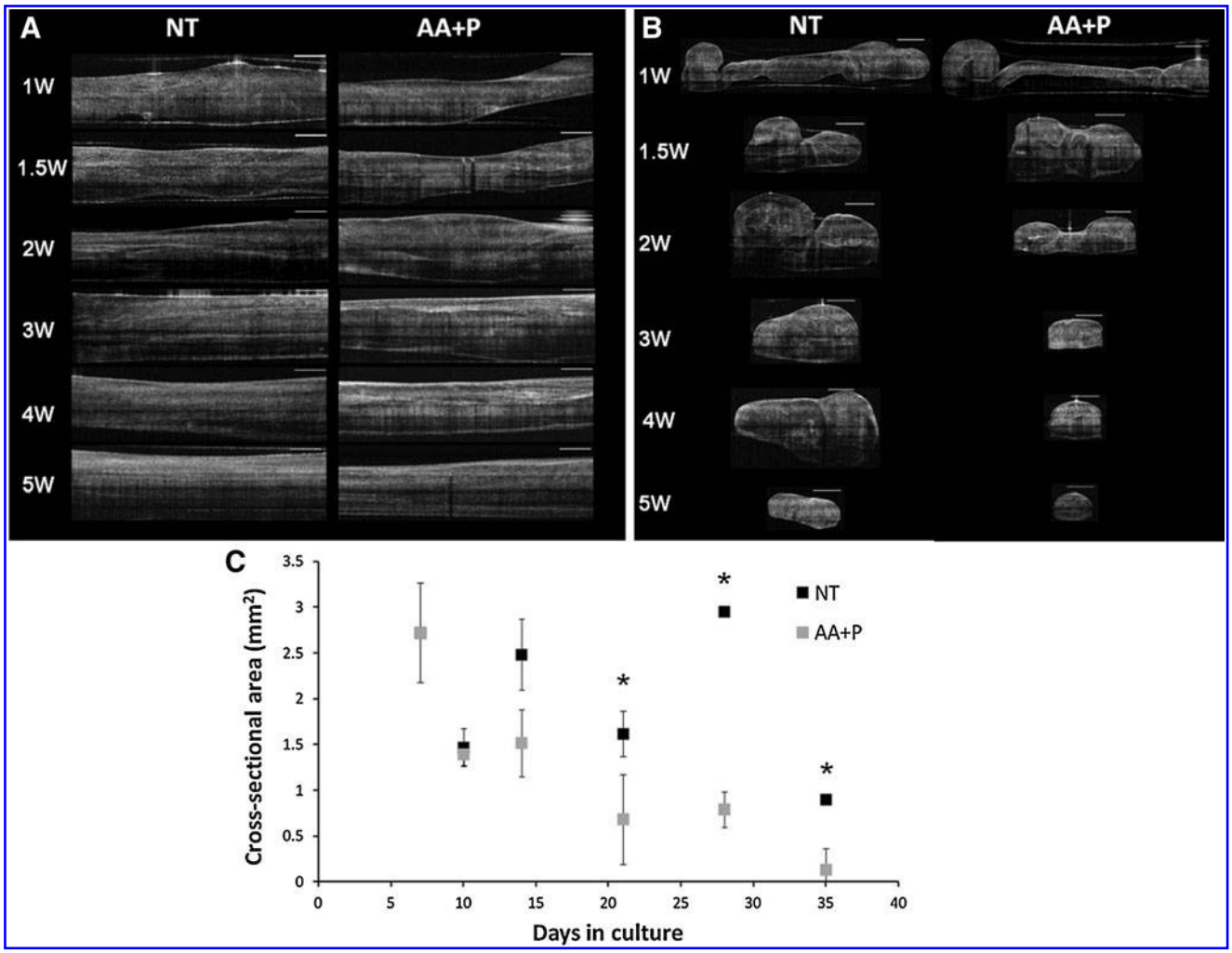

FIG. 5. OCT scans of ligament-like construct maturation: **(A)** longitudinal and **(B)** transverse orientations of the constructs. The difference in the construct morphology on addition of AA + P is evident in the transverse OCT scans. Scale bar represents 1 mm in all images. **(C)** Cross-sectional measurements of ligament-like constructs as measured by ImageJ software. Data are represented as mean ± standard deviation of three measurements per individual scan. $^*p < 0.05$.

22.23 ± 5.49 mm ($p = 0.0045$, ES $r = 0.67$, ES $d = 1.78$). The minimum widths for NT and AA + P were 10.41 ± 4.46 mm and 17.36 ± 7.41 mm, respectively ($p = 0.0275$, ES $r = 0.52$, ES $d = 1.22$). From day 33 to day 52, the average maximum and minimum widths of the NT group were almost double than those of the AA + P group, with the NT group widths being ~1.6 times larger than the AA + P-treated widths (Fig. 8 and Table 1). For example, on day 52, the maximum widths were 2.41 ± 0.48 mm for NT and 1.48 ± 0.15 mm for AA + P, ($p = 0.012$, ES $r = 0.82$, ES $d = 1.63$), while the minimum widths for NT and AA + P were 1.47 ± 0.51 mm and 0.91 ± 0.1 mm, respectively (Fig. 8). All the maximum widths were found to be significant between days 33 and 52 ($p < 0.05$); however, the minimum widths were not. The effect–size statistics,

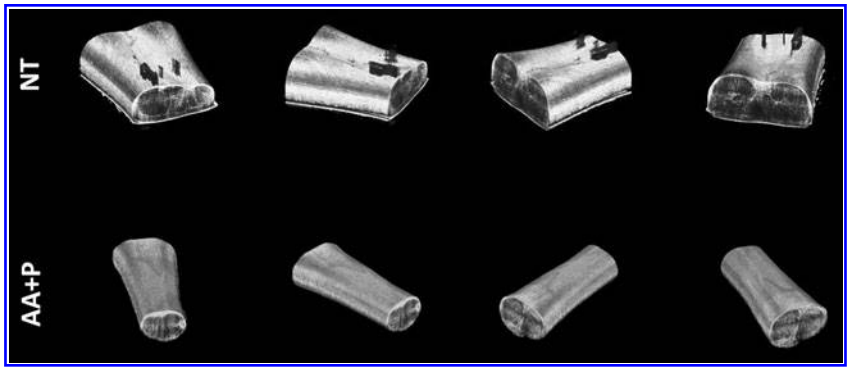

FIG. 6. Three-dimensional reconstructions of the ligament constructs after 2.5 months in culture, with and without AA + P supplementation.

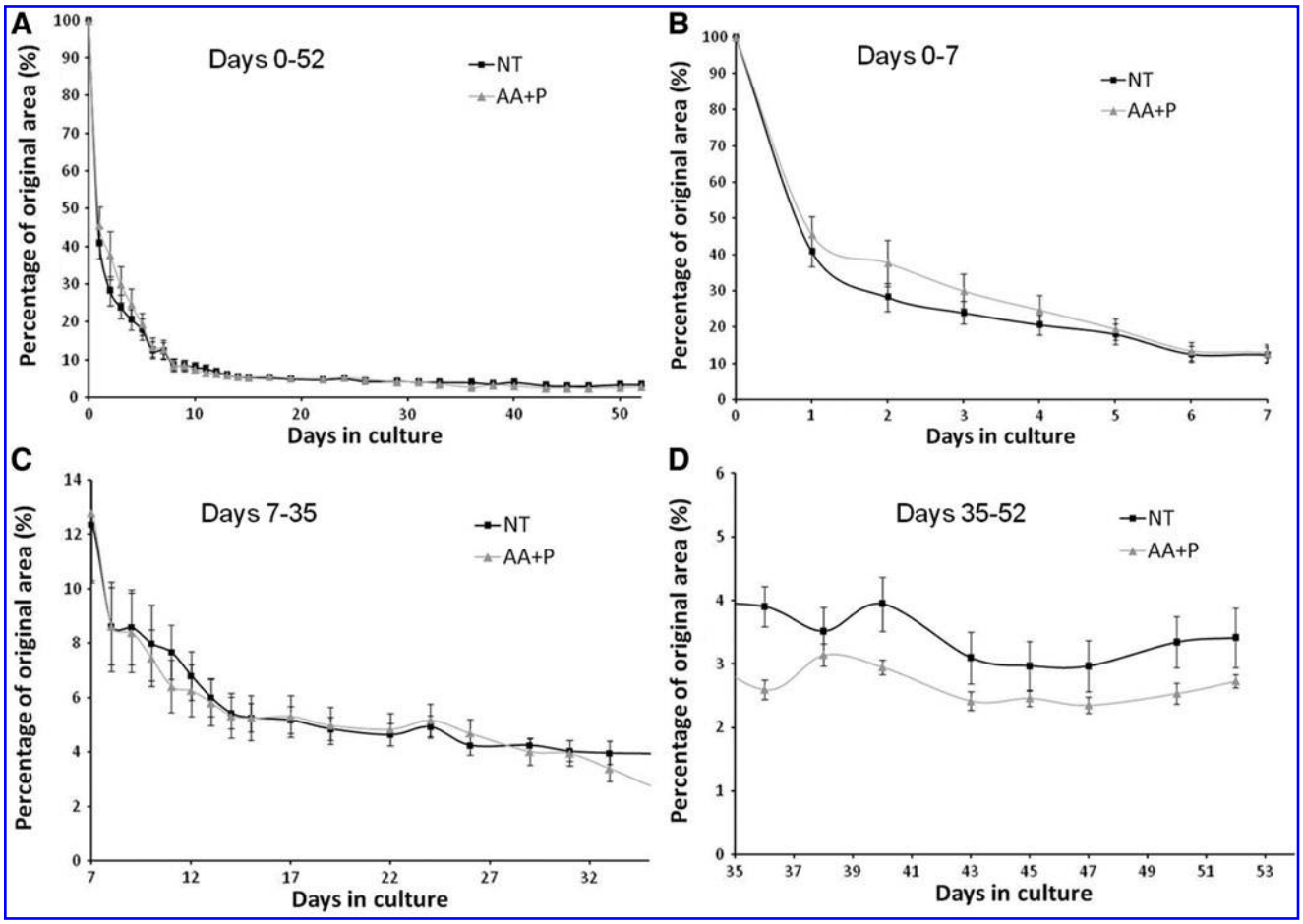

FIG. 7. Quantification of contraction of ligament-like constructs. **(A)** Global percentage reduction in the fibrin gel area over time. **(B)** Early-stage formation of ligament constructs (0–7 days), **(C)** maturation stage (7–35 days), and **(D)** late-stage maturation (35–52 days). $n = 7$ for each time point and group.

which is an indication of the strength of the relationship between the groups, was calculated using Cohen's *d* and Pearson's Correlation Coefficient *r*. Both methods resulted in large effect–size statistical values on day 1 and in the period between days 33 and 52, meaning that although the minimum widths failed to give significant results, there was strong separation between means due to the AA+P treatment (Fig. 8C, D).

The transversal maximum-to-minimum width ratios within each group were also determined to observe if there were any extremes in the construct dimensions (Table 2). Although the magnitude of contraction differed between the groups, the maximum-to-minimum width ratios of the constructs were almost identical by day 52, at 1.64 and 1.62 for NT and AA+P-supplemented, respectively (Table 2). Using the average widths, the aspect ratio of the constructs was calculated (Table 3). The final aspect ratio of the constructs treated with AA+P was larger, at ~10, than for those unsupplemented with an aspect ratio of about 6 (Table 3), again indicating that AA+P changes the final dimensions of the ligament-like constructs.

Histological sections of supplemented ligament-like constructs were taken after 5 and 10 weeks of culture (Fig. 9). H&E staining of the sections shows that in cross section, the folds of the fibrin gel can be seen in the center of the construct (Fig. 9A, small arrows) and where the fibrin gel attaches to the cement anchor (Fig. 9B). Furthermore, a cell layer can be seen on the outside of the tubular structure (Fig. 9A, large arrows) with limited cells visible in the inside of the structure. However, in longitudinal sections at 10 weeks in culture, cells are present throughout the ligament-like construct, and the tissue displayed a fiber-like appearance (Fig. 9C, D). Figure 9C and D also revealed a thick layer on the outer edges of the scaffold, in line with the cortex layer that can be observed in the 3D reconstructions in the AA+P-treated group (Fig. 6).

Discussion

In this study, we have examined the morphological changes occurring during early-stage formation and maturation of tissue-engineered bone-to-bone ligament-like constructs. We have used conventional digital imaging alongside OCT imaging with anticipation that by combining these techniques, we could gain an understanding of construct formation and matrix deposition by nondestructive means, improving our understanding of how these tissues form and develop *in vitro*. Furthermore, we have combined the OCT scans with the digital image analysis of the constructs to study the effect of AA+P supplementation on

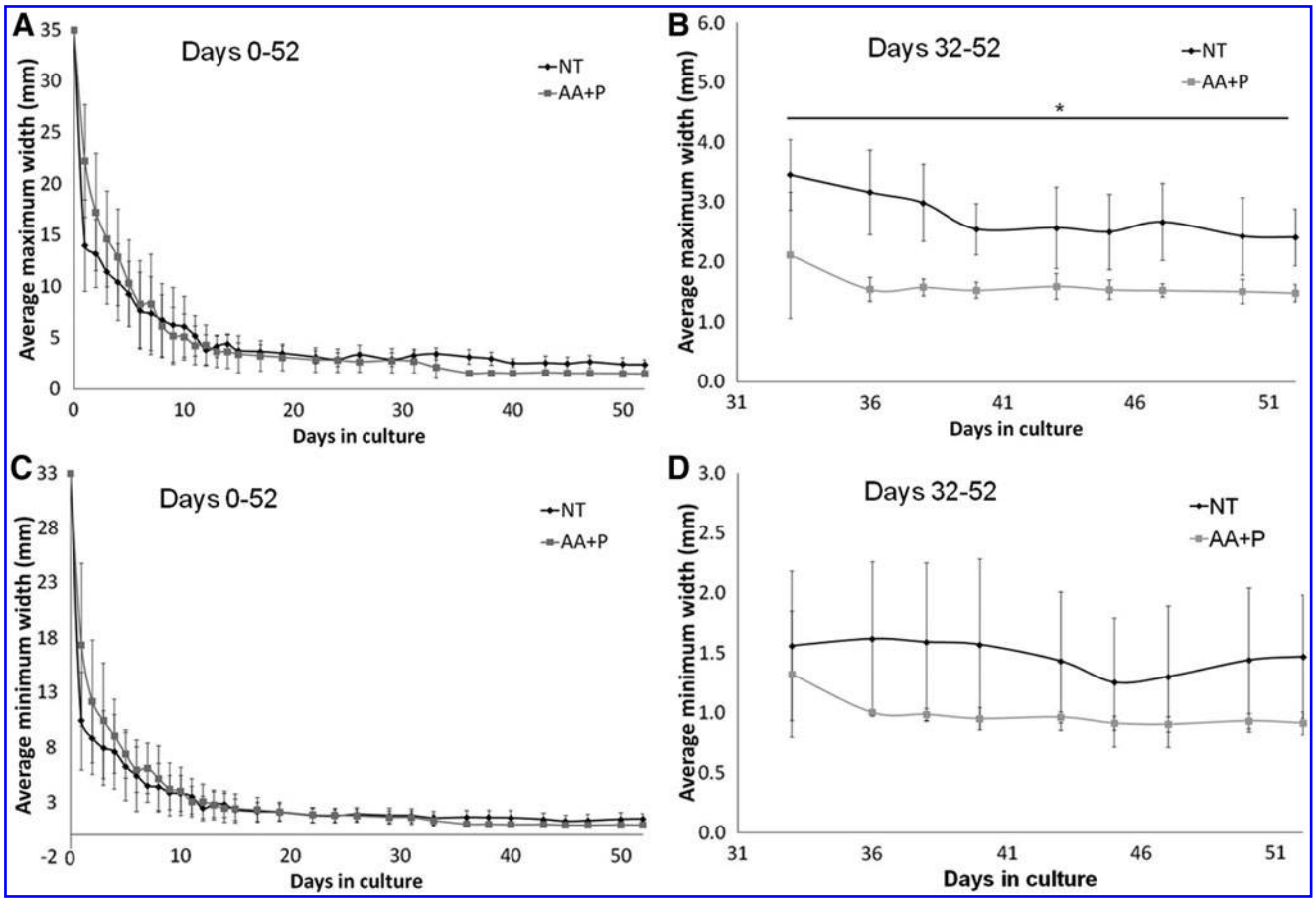

FIG. 8. Transversal maximum and minimum widths of the ligament-like constructs. **(A)** Maximum widths for no treatment (NT) and AA+P constructs over time. **(B)** Maximum widths from 33 to 52 days. **(C)** Minimum widths for NT and AA+P constructs over time. **(D)** Minimum widths from 33 to 52 days. $n=7$ for each time point and group. $^*p<0.05$ between groups.

fibrin gel contraction and tissue-engineered ligament construct formation.

Although the standard histological analysis of tissue-engineered constructs has advantages, such as the ability to determine matrix components and determine cell distribution within tissues, it also has several drawbacks. First, a histological analysis can require the fixation and freezing of tissue constructs. Both these procedures can damage the specimen and therefore may not provide a true representation of tissue morphology. Second, owing to the limitations of light microscopy, constructs need to be sectioned into slices of several micron thicknesses, and therefore it remains difficult to obtain a 3D view of the specimen. This can be problematic if, as is the case here, the gross morphology during formation is of interest. In this study, OCT has allowed an in-depth view of the tissue morphology in both the transverse and the longitudinal orientations that is not possible using digital imaging alone. The use of OCT allowed visualization of the gross cross-sectional morphology of the ligament-like constructs during formation and has permitted a far better understanding of the mode of construct formation. However, it is also apparent that the use of OCT to determine matrix composition by images alone is not ideal and requires further analysis. Some researchers have demonstrated the use of polarization-sensitive OCT to visualize collagen fiber alignment within tendon,[35] cartilage,[36] and tissue-engineered structures.[28] By this method, the polarization of backscattered light is measured after it has passed though the sample, and this can be directly related to the alignment of the collagen fibers. Such an analysis should be performed on the ligament-like construct samples to confirm an increase in

Table 1. Ratio of NT-to-AA+P Maximum and Minimum Widths of Ligament-Like Constructs Over 33–52 Days

		Day								
Description	*Ratio*	*33*	*36*	*38*	*40*	*43*	*45*	*47*	*50*	*52*
Max. width	NT:AA+P	1.63	2.05	1.90	1.67	1.61	1.63	1.75	1.61	1.63
Min. width	NT:AA+P	1.18	1.62	1.62	1.65	1.49	1.38	1.44	1.55	1.61

NT, no treatment; AA+P, ascorbic acid and proline.

Table 2. Ratio of Maximum-to-Minimum Widths of Ligament-Like Constructs in NT- and AA+P-Treated Samples Over 33–52 Days

		Day								
Group	*Ratio*	*33*	*36*	*38*	*40*	*43*	*45*	*47*	*50*	*52*
NT	Max:min	2.22	1.96	1.88	1.62	1.79	1.99	2.05	1.69	1.64
AA+P	Max:min	1.60	1.54	1.60	1.61	1.66	1.69	1.69	1.62	1.62

collagen deposition and alignment in the samples over an extended culture period.

The transverse OCT scans clearly demonstrate the manner in which the fibrin gel contracts around the two anchor points and rolls into a tubular structure (Figs. 2 and 5B). Eventually, the two sides of the construct come into contact and fuse together to form a single longitudinal ligament-like structure by approximately week 2 of culture (Fig. 5B). Another research group has recently reported the formation of tendon-like constructs using a similar method, although they embedded the ACL cells into the fibrin gel before polymerization.[37] It would also be interesting to compare the methods of formation of those constructs using OCT, to establish their mode of formation. Furthermore, it seems likely that the two modes of formation could result in a distinct mechanical behavior between the two and may provide evidence to establish which method is conducive to forming engineered tissues with greater mechanical integrity.

The decision to supplement the ligament-like constructs with AA+P was made through our previous work that demonstrates that the addition of AA+P to the culture media of the constructs resulted in an increased deposition of collagen within the fibrin matrix after only 1 week of supplementation.[11] As expected, the supplementation of AA+P over the 5-week culture period resulted in a continuous increase in the collagen content of the constructs (Fig. 4A). AA is an essential cofactor for prolyl-4-hydroxylase, and its presence is required for the hydroxylation of collagen chains during collagen fibril assembly.[38] In addition, as proline is a major constituent of the collagen protein, it is not surprising that increasing both AA and proline availability augments collagen production. Here, we have also demonstrated the effect that AA+P supplementation has on contraction of the ligament-like constructs, with supplemented groups displaying increased contraction in the digital images (Fig. 3), OCT scans (Fig. 5B), and the evaluation of contraction by digital imaging (Figs. 7 and 8). Although there were no statistically significant differences between the gel areas of the NT- and AA+P-supplemented constructs, the maximum widths of the constructs differed significantly between the groups between days 33 and 52 (Fig. 8B). The ratios calculated from the results (Table 1) do show that there is some inherent pattern in the formation of the constructs with regard to the maximum and minimum widths achieved. The ratios of the maximum-to-minimum width of the supplemented group appeared to stabilize from day 33 onward, at a value of about 1.6. The max/min ratio for the NT group is not as consistent, but reaches a similar value of 1.64 on day 52. A possible explanation for the stability seen in the max/min ratio of the AA+P group, in the final stages of the study, could be that treatment with AA+P causes a more uniform and controlled type of contraction of the gel as a result of increased deposition of collagen matrix (Fig. 4A).

However, it must also be noted that with the digital images and resulting contraction data, the area measured does not take the depth of the construct into account. As observed in the transverse OCT scans, AA+P-supplemented constructs display distinct cross-sectional areas (Fig. 5B) with unsupplemented constructs remaining broad and flat and AA+P-supplemented constructs becoming thin and round. Cross-sectional area was less in supplemented constructs than in unsupplemented constructs from day 14 onward (Fig. 5C) reaching values of 0.132 and 0.9 mm^2 respectively at the 35-day time point (Fig. 5C). Native ligaments are typically described as broad, flat tissues; in particular, the ACL has an average length and width range in humans from 22 to 41 mm and 7 to 12 mm, respectively.[39] Based on this information, although collagen content improves, the increased contraction observed on addition of AA+P is not ideal for our intended application, as it results in the production of thin, tubular structures, vastly different from the native ligament tissue morphology. The fact that supplemented constructs display greater contraction is not unexpected, since AA addition has been shown to increase wound contraction in mouse[40] and guinea pig models.[41–43] It is important to note that even though the AA+P constructs contract to a greater degree, the dry weight of the constructs does not significantly differ at any time point (Fig. 4B). Furthermore, it is critical to mention that while the cross-sectional area of the construct was measured, these measures were made at only one point in the graft. In hindsight, since the constructs are not completely uniform, it would have been beneficial to obtain several scans along the full length of the construct. Future work should focus on obtaining a

Table 3. Ratio of Length to Width of Ligament-Like Constructs in NT and AA+P Samples Over 33–52 Days

		Day								
Group	*Ratio*	*33*	*36*	*38*	*40*	*43*	*45*	*47*	*50*	*52*
NT	Length:width	4.79	5.03	5.25	5.84	6.01	6.40	6.06	6.22	6.20
AA+P	Length:width	7.18	9.71	9.64	9.96	9.66	10.08	10.18	10.13	10.32

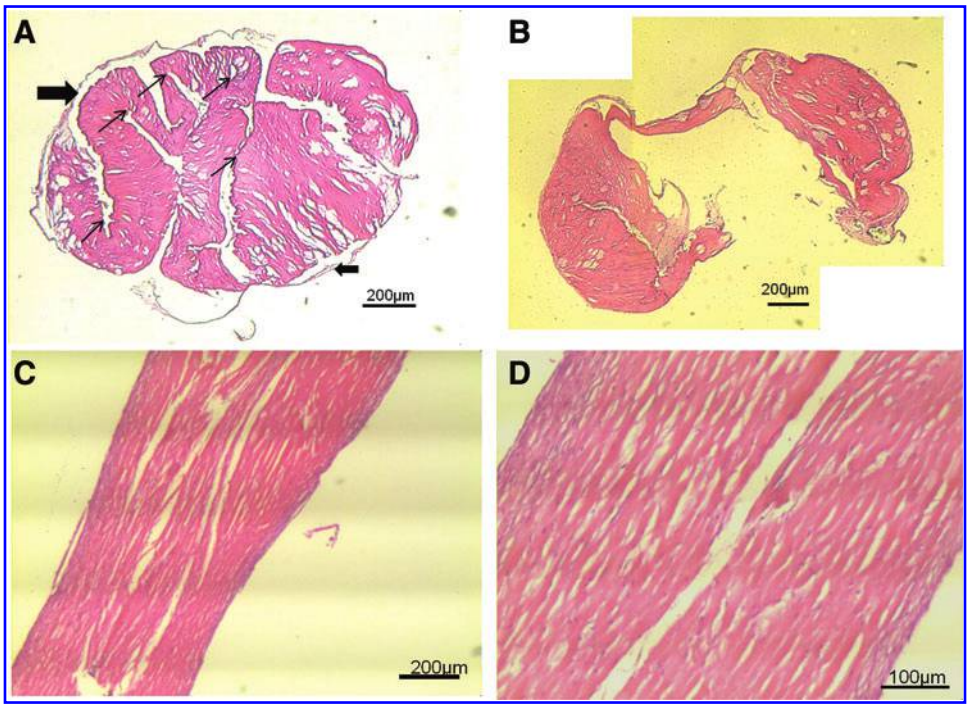

FIG. 9. Histological sections of AA+P-treated ligament-like constructs. **(A)** Transverse section from the midpoint of an AA+P-treated sample after 5 weeks in culture. The folds of the fibrin can be seen clearly (small arrows). Also, a cell layer is present on the outside of the tubular scaffold (large arrows). Stained with hematoxylin and eosin. **(B)** Transverse section of an AA+P-treated sample after 5 weeks in culture taken from the end of the construct near the cement anchor point. The midpoints of the construct have not joined together, probably due to the mechanical barrier of the cement anchor. **(C, D)** Longitudinal section of an AA+P-treated construct after 10 weeks in culture. Cell nuclei (blue) are distributed throughout the fibrous scaffold (pink), although are seen to be more prominent on the outer layers, creating a thick, dense layer on either side of the construct. Cells appear to align in the direction of tension. Color images available online at www.liebertonline.com/tea

complete scan along the length of the construct, since the morphological tapering evident in the digital images (Fig. 3) and the 3D reconstructions (Fig. 6) was not taken into account when the scans were collected. This inaccuracy in obtaining scans likely explains the variability of the cross-sectional area data and the large increase in the cross-sectional area at the 4-week time point in the unsupplemented group (Fig. 5C).

The mechanism for increased contraction in the ligament-like constructs on addition of AA+P could be multifaceted. As mentioned, exogenous addition of both AA+P lead to improved collagen accumulation; therefore, it is possible that by increasing the collagen content, collagen fibrils act to contract the fibrin matrix further as they crosslink with one another under control of the enzyme lysyl oxidase. However, contrary to this, a 1-mM dose of AA has been shown to have an inhibitory effect on lysyl oxidase activity *in vitro*,[44] although the authors performed no further experiments to establish the inhibitory ranges of AA concentrations. Furthermore, AA has been shown to have positive and negative effects on cellular proliferation depending on cell type. One reason for increased contraction could be an increase in cell number and therefore faster cell-mediated enzymatic digestion of the initial fibrin matrix. We have previously shown that 1 week of 50 μM AA+P supplementation increases the embryonic chick tendon fibroblasts cell number within the constructs.[11] Conversely, AA may act to transdifferentiate fibroblasts into a contractile myofibroblastic phenotype, with cells rich in α-smooth muscle actin as reported in smooth muscle cells[45,46] and bone mesenchymal stem cells.[47] This has been previously been reported to occur in fibroblasts on addition of transforming growth factor-β,[48] a growth factor pivotal to the collagen fibrillogenesis pathway, so it is possible that a related effect is occurring within our system. In two dimensions, addition of 250 μM AA+ 50 μM P to our fibroblast culture resulted in no significant change in the cell number (data not shown); however, since the attachment to the external environment in 2D is very different from that in 3D,[49] no conclusions can be drawn without further analysis within this tissue-engineered ligament system.

The histological analysis shows that cells populate the entire scaffold and align in the direction of tension (Fig. 9). Also, taken with the 3D scans of the ligament constructs, the formation of a dense, outer cortex can be seen (Figs. 6 and 8). Another research group has used immunohistochemical techniques to investigate the deposition of extracellular matrix (ECM) using ACL cells in this fibrin gel system.[37] Interestingly, they showed that a cortex of collagen type I was formed with mainly collagen type XII in the core of the construct.[37] Our hydroxyproline content assay does not distinguish between types of collagen, so we are currently undertaking work to give a full immunohistochemical analysis of the ECM deposited over the culture period. It may be that the mechanical environment predisposes the production of different types of collagen, and it is important to establish what these matrix proteins are within this system.

It is also likely that addition of AA+P affects matrix metalloproteinase (MMP) activity. MMPs are a family of zinc-dependent proteases that degrade components of the ECM.[50,51] Also, members of the A disintegrin and metalloproteinases with the thrombospondin motif (ADAMTS) family, known as the aggrecanases, act to degrade proteoglycans within the ECM,[52] and the enzymatic activity of both MMPs and ADAMTS is central to the control of matrix remodeling. Also, the tissue inhibitors of MMPs act to inhibit the degradative functions of MMPs in an effort to maintain homeostasis within the ECM.[27,53] Although the expression of quantification of MMP was not performed in the current study, the effect of AA+P on control of MMP activity remains an important factor to understand with regard to formation and contraction of the ligament-like constructs. Analysis of MMP will form part of our future work on this system.

Conclusions

This study has used digital imaging techniques, OCT, and histology to monitor the early-stage formation and maturation of tissue-engineered ligament-like constructs. OCT has allowed a complete cross-sectional view of the constructs during formation and the gross contraction of the fibrin-based cultures. It has also been shown that although AA+P supplementation continues to significantly improve collagen production over a 5-week period, it also causes excessive contraction of the constructs, producing a thin, round cross-sectional morphology rather than broad, flat ligament-like tissues that could prove problematic for our intended application as ACL replacement. Further analysis of effect of supplementation on the contraction method is crucial for the future development of tissue-engineered ligaments with clinically relevant morphological characteristics for implantation.

Acknowledgments

The authors would like to thank Dr. Keith Baar for his helpful comments during preparation of the article. We would also like to acknowledge the BBSRC for funding this work (Project number BB/G022356/1).

Disclosure Statement

No competing financial interests exist.

References

1. Cimino, F., Volk, B.S., and Setter, D. Anterior cruciate ligament injury: diagnosis, management, and prevention. Am Fam Physician **82,** 917, 2010.
2. Clayton, R.A., and Court-Brown, C.M. The epidemiology of musculoskeletal tendinous and ligamentous injuries. Injury **39,** 1338, 2008.
3. Benjaminse, A., Gokeler, A., and van der Schans, C.P. Clinical diagnosis of an anterior cruciate ligament rupture: a meta-analysis. J Orthop Sports Phys Ther **36,** 267, 2006.
4. Chang, S.K., Egami, D.K., Shaieb, M.D., Kan, D.M., and Richardson, A.B. Anterior cruciate ligament reconstruction: allograft versus autograft. Arthroscopy **19,** 453, 2003.
5. Louboutin, H., Debarge, R., Richou, J., Selmi, T.A., Donell, S.T., Neyret, P., *et al.* Osteoarthritis in patients with anterior cruciate ligament rupture: a review of risk factors. Knee **16,** 239, 2009.
6. Chaudhari, A.M., Briant, P.L., Bevill, S.L., Koo, S., and Andriacchi, T.P. Knee kinematics, cartilage morphology, and osteoarthritis after ACL injury. Med Sci Sports Exerc **40,** 215, 2008.
7. Kartus, J., Movin, T., and Karlsson, J. Donor-site morbidity and anterior knee problems after anterior cruciate ligament reconstruction using autografts. Arthroscopy **17,** 971, 2001.
8. Kartus, J., Stener, S., Lindahl, S., Engstrom, B., Eriksson, B.I., and Karlsson, J. Factors affecting donor-site morbidity after anterior cruciate ligament reconstruction using bone-patellar tendon-bone autografts. Knee Surg Sports Traumatol Arthrosc **5,** 222, 1997.
9. Mascarenhas, R., and MacDonald, P.B. Anterior cruciate ligament reconstruction: a look at prosthetics—past, present and possible future. Mcgill J Med **11,** 29, 2008.
10. Mastrokalos, D.S., Springer, J., Siebold, R., and Paessler, H.H. Donor site morbidity and return to the preinjury activity level after anterior cruciate ligament reconstruction using ipsilateral and contralateral patellar tendon autograft: a retrospective, nonrandomized study. Am J Sports Med **33,** 85, 2005.
11. Paxton, J.Z., Grover, L.M., and Baar, K. Engineering an *in vitro* model of a functional ligament from bone to bone. Tissue Eng Part A **16,** 3515, 2010.
12. Hsiung, P.L., Phatak, D.R., Chen, Y., Aguirre, A.D., Fujimoto, J.G., and Connolly, J.L. Benign and malignant lesions in the human breast depicted with ultrahigh resolution and three-dimensional optical coherence tomography. Radiology **244,** 865, 2007.
13. Zhou, C., Cohen, D.W., Wang, Y., Lee, H.C., Mondelblatt, A.E., Tsai, T.H., *et al.* Integrated optical coherence tomography and microscopy for *ex vivo* multiscale evaluation of human breast tissues. Cancer Res **70,** 10071, 2010.
14. Larin, K.V., Larina, I.V., Liebling, M., and Dickinson, M.E. Live Imaging of early developmental processes in mammalian embryos with optical coherence tomography. J Innov Opt Health Sci **2,** 253, 2009.
15. Larina, I.V., Furushima, K., Dickinson, M.E., Behringer, R.R., and Larin, K.V. Live imaging of rat embryos with Doppler swept-source optical coherence tomography. J Biomed Opt **14,** 050506. 2009.
16. Boppart, S.A., Tearney, G.J., Bouma, B.E., Southern, J.F., Brezinski, M.E., and Fujimoto, J.G. Noninvasive assessment of the developing Xenopus cardiovascular system using optical coherence tomography. Proc Natl Acad Sci U S A **94,** 4256, 1997.
17. Davlouros, P.A., Mavronasiou, E., Xanthopoulou, I., Karantalis, V., Tsigkas, G., Hahalis, G., *et al.* An optical coherence tomography study of two new generation stents with biodegradable polymer carrier, eluting paclitaxel vs. biolimus-A9. Int J Cardiol 2011 [Epub ahead of print]; DOI: 10.1016/j.ijcard.2010.12.072.
18. Greenberg, B.M., and Frohman, E. Optical coherence tomography as a potential readout in clinical trials. Ther Adv Neurol Disord **3,** 153, 2010.
19. Mansoori, T., Viswanath, K., and Balakrishna, N. Reproducibility of peripapillary retinal nerve fibre layer thickness measurements with spectral domain optical coherence tomography in normal and glaucomatous eyes. Br J Ophthalmol **95,** 685, 2011.
20. Drexler, W., Morgner, U., Ghanta, R.K., Kartner, F.X., Schuman, J.S., and Fujimoto, J.G. Ultrahigh-resolution ophthalmic optical coherence tomography. Nat Med **7,** 502, 2001.
21. Liang, X., Graf, B.W., and Boppart, S.A. Imaging engineered tissues using structural and functional optical coherence tomography. J Biophotonics **2,** 643, 2009.

22. Bagnaninchi, P.O., Yang, Y., Zghoul, N., Maffulli, N., Wang, R.K., and Haj, A.J. Chitosan microchannel scaffolds for tendon tissue engineering characterized using optical coherence tomography. Tissue Eng **13,** 323, 2007.
23. Chen, C.W., Betz, M.W., Fisher, J.P., Paek, A., and Chen, Y. Macroporous hydrogel scaffolds and their characterization by optical coherence tomography. Tissue Eng Part C Methods 2010 [Epub ahead of print]; DOI: 10.1089/ten.tec.2010.0072.
24. Zheng, K., Rupnick, M.A., Liu, B., and Brezinski, M.E. Three dimensional OCT in the engineering of tissue constructs: a potentially powerful tool for assessing optimal scaffold structure. Open Tissue Eng Regen Med J **2,** 8, 2009.
25. Aydin, H.M., El Haj, A.J., Piskin, E., and Yang, Y. Improving pore interconnectivity in polymeric scaffolds for tissue engineering. J Tissue Eng Regen Med **3,** 470, 2009.
26. Smith, L.E., Bonesi, M., Smallwood, R., Matcher, S.J., and MacNeil, S. Using swept-source optical coherence tomography to monitor the formation of neo-epidermis in tissue-engineered skin. J Tissue Eng Regen Med **4,** 652, 2010.
27. Levitz, D., Hinds, M.T., Ardeshiri, A., Hanson, S.R., and Jacques, S.L. Non-destructive label-free monitoring of collagen gel remodeling using optical coherence tomography. Biomaterials **31,** 8210, 2010.
28. Ahearne, M., Bagnaninchi, P.O., Yang, Y., and El Haj, A.J. Online monitoring of collagen fibre alignment in tissue-engineered tendon by PSOCT. J Tissue Eng Regen Med **2,** 521, 2008.
29. Paxton, J.Z., Donnelly, K., Keatch, R.P., Baar, K., and Grover, L.M. Factors affecting the longevity and strength in an *in vitro* model of the bone-ligament interface. Ann Biomed Eng **38,** 2155, 2010.
30. Edwards, C.A., and O'Brien, W.D., Jr. Modified assay for determination of hydroxyproline in a tissue hydrolyzate. Clin Chim Acta **104,** 161, 1980.
31. Neuman, R.E., and Logan, M.A. The determination of hydroxyproline. J Biol Chem **184,** 299, 1950.
32. Stricker, D. BrightStat.com: free statistics online. Comput Methods Programs Biomed **92,** 135, 2008.
33. Cohen, J. A power primer. Psychol Bull **112,** 155, 1992.
34. Nakagawa, S., and Cuthill, I.C. Effect size, confidence interval and statistical significance: a practical guide for biologists. Biol Rev Camb Philos Soc **82,** 591, 2007.
35. Bagnaninchi, P.O., Yang, Y., Bonesi, M., Maffulli, G., Phelan, C., Meglinski, I., *et al.* In-depth imaging and quantification of degenerative changes associated with Achilles ruptured tendons by polarization-sensitive optical coherence tomography. Phys Med Biol **55,** 3777, 2009.
36. Ugryumova, N., Jacobs, J., Bonesi, M., and Matcher, S.J. Novel optical imaging technique to determine the 3-D orientation of collagen fibers in cartilage: variable-incidence angle polarization-sensitive optical coherence tomography. Osteoarthritis Cartilage **17,** 33, 2009.
37. Bayer, M.L., Yeung, C.Y., Kadler, K.E., Qvortrup, K., Baar, K., Svensson, R.B., *et al.* The initiation of embryonic-like collagen fibrillogenesis by adult human tendon fibroblasts when cultured under tension. Biomaterials **31,** 4889, 2010.
38. Kadler, K.E., Baldock, C., Bella, J., and Boot-Handford, R.P. Collagens at a glance. J Cell Sci **120,** 1955, 2007.
39. Girgis, F.G., Marshall, J.L., and Monajem, A. The cruciate ligaments of the knee joint. Anatomical, functional and experimental analysis. Clin Orthop Relat Res 216, 1975.
40. Jagetia, G.C., Rajanikant, G.K., and Rao, S.K. Evaluation of the effect of ascorbic acid treatment on wound healing in mice exposed to different doses of fractionated gamma radiation. Radiat Res **159,** 371, 2003.
41. Jagetia, G.C., Rajanikant, G.K., Mallikarjun, and Rao, K.V. Ascorbic acid increases healing of excision wounds of mice whole body exposed to different doses of gamma-radiation. Burns **33,** 484, 2007.
42. Cabbabe, E.B., and Korock, S.W. Wound healing in vitamin C-deficient and nondeficient guinea pigs: a pilot study. Ann Plast Surg **17,** 330, 1986.
43. Silverstein, R.J., and Landsman, A.S. The effects of a moderate and high dose of vitamin C on wound healing in a controlled guinea pig model. J Foot Ankle Surg **38,** 333, 1999.
44. Kuroyanagi, M., Shimamura, E., Kim, M., Arakawa, N., Fujiwara, Y., and Otsuka, M. Effects of L-ascorbic acid on lysyl oxidase in the formation of collagen cross-links. Biosci Biotechnol Biochem **66,** 2077, 2002.
45. Kim, P.D., Peyton, S.R., VanStrien, A.J., and Putnam, A.J. The influence of ascorbic acid, TGF-beta1, and cell-mediated remodeling on the bulk mechanical properties of 3-D PEG-fibrinogen constructs. Biomaterials **30,** 3854, 2009.
46. Arakawa, E., Hasegawa, K., Irie, J., Ide, S., Ushiki, J., Yamaguchi, K., *et al.* L-ascorbic acid stimulates expression of smooth muscle-specific markers in smooth muscle cells both *in vitro* and *in vivo*. J Cardiovasc Pharmacol **42,** 745, 2003.
47. Narita, Y., Yamawaki, A., Kagami, H., Ueda, M., and Ueda, Y. Effects of transforming growth factor-beta 1 and ascorbic acid on differentiation of human bone-marrow-derived mesenchymal stem cells into smooth muscle cell lineage. Cell Tissue Res **333,** 449, 2008.
48. Desmouliere, A., Geinoz, A., Gabbiani, F., and Gabbiani, G. Transforming growth factor-beta 1 induces alpha-smooth muscle actin expression in granulation tissue myofibroblasts and in quiescent and growing cultured fibroblasts. J Cell Biol **122,** 103, 1993.
49. Cukierman, E., Pankov, R., Stevens, D.R., and Yamada, K.M. Taking cell-matrix adhesions to the third dimension. Science **294,** 1708, 2001.
50. Bedi, A., Kovacevic, D., Hettrich, C, Gulotta, L.V., Ehteshami, J.R., Warren, R.F., *et al.* The effect of matrix metalloproteinase inhibition on tendon-to-bone healing in a rotator cuff repair model. J Shoulder Elbow Surg **19,** 384, 2010.
51. Nagase, H., Visse, R., and Murphy, G. Structure and function of matrix metalloproteinases and TIMPs. Cardiovasc Res **69,** 562, 2006.
52. Riley, G. Tendinopathy—from basic science to treatment. Nat Clin Pract Rheumatol **4,** 82, 2008.
53. Karousou, E., Ronga, M., Vigetti, D., Passi, A., and Maffulli, N. Collagens, proteoglycans, MMP-2, MMP-9 and TIMPs in human achilles tendon rupture. Clin Orthop Relat Res **466,** 1577, 2008.

Address correspondence to:
Jennifer Z. Paxton, Ph.D.
School of Chemical Engineering
College of Physical Sciences and Engineering
University of Birmingham
Edgbaston
Birmingham B15 2TT
United Kingdom

E-mail: jzpaxton.research@gmail.com

Received: September 22, 2011
Accepted: March 16, 2012
Online Publication Date: May 17, 2012

This article has been cited by:

1. U. N. G. Wudebwe, A. Bannerman, P. Goldberg-Oppenheimer, J. Z. Paxton, R. L. Williams, L. M. Grover. 2014. Exploiting cell-mediated contraction and adhesion to structure tissues in vitro. *Philosophical Transactions of the Royal Society B: Biological Sciences* **370**, 20140200-20140200. [CrossRef]
2. Pilar de la Puente, Dolores Ludeña. 2014. Cell culture in autologous fibrin scaffolds for applications in tissue engineering. *Experimental Cell Research* **322**, 1-11. [CrossRef]
3. Susanne Koburger, Alistair Bannerman, Liam M. Grover, Frank A. Müller, James Bowen, Jennifer Z. Paxton. 2014. A novel method for monitoring mineralisation in hydrogels at the engineered hard–soft tissue interface. *Biomaterials Science* . [CrossRef]
4. Susanne Koburger, Alistair Bannerman, Liam M. Grover, Frank A. Müller, James Bowen, Jennifer Z. Paxton. 2014. A novel method for monitoring mineralisation in hydrogels at the engineered hard–soft tissue interface. *Biomater. Sci.* **2**, 41-51. [CrossRef]
5. Paul Hagerty, Ann Lee, Sarah Calve, Cassandra A. Lee, Martin Vidal, Keith Baar. 2012. The effect of growth factors on both collagen synthesis and tensile strength of engineered human ligaments. *Biomaterials* **33**, 6355-6361. [CrossRef]